Nanoordering of Fluorinated Side-Chain Liquid Crystalline/Amorphous Diblock Copolymers

M. Al-Hussein,[†,⊥] Y. Séréro,[†] O. Konovalov,[‡] A. Mourran,[§] M. Möller,[§] and W. H. de Jeu*[,†]

FOM-Institute for Atomic and Molecular Physics, Kruislaan 407, 1098 SJ Amsterdam, The Netherlands; ID10B, European Synchrotron Radiation Facility, BP 220, 38043 Grenoble, France; and DWI, RWTH Aachen, Pauwelstrasse 8, 52074 Aachen, Germany

Received May 10, 2005; Revised Manuscript Received August 29, 2005

ABSTRACT: The role of anchoring the mesogenic side chains at the internal and boundary interfaces in the thin film morphology has been investigated for two fluorinated side-chain liquid crystalline/amorphous diblock copolymers. Initial bulk investigations indicate that the two polymers strongly microphase segregate into a cylindrical and a lamellar morphology, respectively. Inside the liquid-crystal block, the cylinder-forming block copolymer shows both a crystalline-B and a smectic-A phase, whereas the lamellae-forming polymer gives only a smectic-A phase, with the side chains organized in double layers with a spacing of 3.33 nm. In both situations the smectic layers are oriented perpendicular to the block interfaces, which state is retained in films. In thin films of the cylinder-forming block copolymer, the smectic layering and the orientational wetting properties of the fluorinated side chains stabilize the minority cylindrical domains normal to the substrate. For films of the lamellar system, however, an evolved structure forms with block lamellae parallel to the substrate in combination with anchoring of the fluorinated chains at the surface of the film.

1. Introduction

Side-chain liquid-crystalline diblock copolymers (SCLC-BCs) are a special class of soft matter with various potential applications in the field of nanotechnology. They combine blocks of a polymer with mesogenic side groups and of a conformationally isotropic polymer. Some early reviews are given in refs 1−3. Their microstructure is formed under the influence of two driving forces: liquid-crystalline (LC) ordering of the mesogens and the microphase separation (interblock incompatibility). The interplay between these two self-organizing mechanisms can lead to different morphologies than expected for their amorphous copolymers counterparts. Equally well, the LC phase behavior may be influenced by the confinement in microdomains.[4−12] The ability of SCLC-BCs to simultaneously organize on different length scales can be exploited to tailor material properties.[13,14]

In thin films of block copolymers, additional driving forces for structure formation come to play.[15] Generally, the block with the lowest surface energy preferentially accumulates at the air surface and the block with the lowest interfacial energy at the substrate. The presence of such surface field and the confinement of the material in thin films often results in a large-scale alignment of the microdomains and stabilization of novel morphologies. In the case of SCLC-BCs, anchoring of the mesogens at the internal microdomain interfaces and at the film boundary surfaces (orientational wetting) plays an additional role in the ordering process.[16,17] This anchoring may be planar, homeotropic, or at some angle to the interface. These extra factors provide further handles to manipulate the order and orientation of the microdomains in thin films.

In this work, we focus on the role of mesogen anchoring in the structure formation of a SCLC-BC. The system studied is a diblock copolymer made of a poly(methyl methacrylate) (PMMA) block and a poly(acrylate) block bearing semifluorinated alkyl side chains. The side chain is a phenyl-free rigid mesogen with a strong tendency to form a smectic phase. In comparison to LC-amorphous block copolymers with conventional side group mesogens, fluorinated side-chain block copolymers exhibit a more pronounced ability to organize as a result of their intrinsic low surface energy.[18,19] Fluorinated block copolymers have potential applications as surface modifiers with useful properties as water and oil repellents because of their biocompatibility and because of nonstick behavior due to their low surface energy character.[20−28] Thus, the ordering of such systems is induced by the thermodynamic interactions between the fluorinated block, the amorphous one, and the surface, which strongly favors surface segregation of the fluorinated block. We have used a couple of semifluorinated diblock copolymers with cylindrical and lamellar morphologies in the bulk and thin films. The bulk phase behavior has been probed by simultaneous small- and wide-angle X-ray scattering (SAXS/WAXS), while in thin films a combination of atomic force microscopy (AFM), X-ray reflectivity (XR), and grazing-incidence X-ray diffraction (GIXD) provided essentially a complete characterization of the nanostructures. In all cases the smectic layers were found to orient perpendicular to the block interfaces. The anchoring of the fluorinated chains at the film boundaries led to smectic layering parallel to the substrate and thus stabilized perpendicular cylinders. For the lamellar morphology the thin film structure was more intricate.

[†] FOM-Institute for Atomic and Molecular Physics.
[‡] European Synchrotron Radiation Facility.
[§] DWI, RWTH Aachen.
[⊥] Present address: The University of Jordan, Physics Department, Amman, Jordan.
* Corresponding author. E-mail: dejeu@amolf.nl.

10.1021/ma050972x CCC: $30.25
Published on Web 10/15/2005

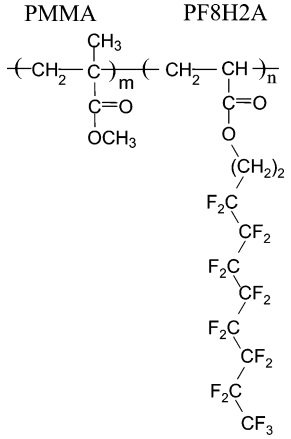

Figure 1. Molecular structure of the diblock copolymers.

2. Experimental Section

2.1. Samples. Two diblock copolymers of the structure shown in Figure 1, with different molecular weights and volume fractions, were synthesized using atom transfer radical polymerization as described elsewhere.[22] Their characteristics are listed in Table 1. The liquid-crystalline block is poly(1*H*,1*H*,2*H*,2*H*-perfluorodecyl acrylate) (PF8H2A) while the amorphous block is poly(methyl methacrylate) (PMMA). Bulk samples were investigated after melting and heating to 170 °C for 10 min; subsequently, they were cooled slowly to room temperature. Films of F1 and F2 were spin-coated from solutions of 1,1,2-trichlorotrifluoroethane onto a Si wafer. The copolymer concentration ranged between 10 and 40 g/L while the speed and the duration of the spinning process were 2000 rpm and 30 s, respectively, leading to a thickness between tens and hundreds of nanometers. The films were dried and subsequently annealed at 170 °C. Note that this is well above T_{Ai}, the smectic-A−isotropic transition temperature.

2.2. Atomic Force Microscopy. The surface morphology of the thin films was investigated by atomic force microscopy (AFM) at room temperature using either a Solver SFM (NT-MDT, Zelenograd, Moscow) or a Digital Instrument Multimode scanning force microscope equipped with a Nanoscope IIIa controller. Imaging was done in the tapping mode using standard silicon cantilevers with a resonant frequency of about 300 kHz and a silicon tip with a curvature radius of 10 nm and a spring constant of 42 N/m.

2.3. Small- and Wide-Angle X-ray Scattering. Small- and wide-angle X-ray scattering (SAXS and WAXS) was performed using an in-house setup with a rotating anode X-ray generator (Rigaku RU-H300) operating at 18 kW. By employing two graded parabolic multilayer mirrors (Bruker, Karlsruhe), a highly parallel beam of monochromatic Cu Kα radiation (λ = 0.154 nm) with a divergence of 0.012° was obtained. A Linkam CSS450 cell was used as temperature-controlled sample stage. The SAXS patterns were recorded with a Bruker Hi-Star area detector at two sample-to-detector distances: 0.37 and 1.03 m. The two-dimensional scattering patterns were circularly integrated, corrected for background, and displayed as one-dimensional plots of the intensity as a function of $q = (4\pi/\lambda)\sin\theta$, the modulus of the scattering vector **q**, in which 2θ is the scattering angle. The WAXS data were recorded using a linear position-sensitive detector (PSD-50M, Braun).

2.4. X-ray Reflectivity. For in-house X-ray reflectivity (XR) measurements the Cu Kα radiation was collimated by a W/B_4C graded parabolic multilayer mirror (Osmic, Auburn Hills, MI) in the scattering plane only (*xz*-plane with the *z*-axis along the film normal, see Figure 2). The samples were mounted vertically at the center of a two-circle goniometer and investigated under specular reflection conditions. Additional presample and predetector slits resulted in an overall resolution in the horizontal scattering plane of $\Delta q_z = 0.03$ nm^{-1}. The intensity was integrated over the broad resolution in the vertical *y*-direction. In reciprocal space specular reflectivity scans probe the scattered intensity along q_z. The X-ray intensity was corrected for sample size effects at small incidence angles as well as for background scattering. The data were analyzed using an iterative matrix formalism derived from the Fresnel equations, taking the deviations from the ideal decay of the reflectivity for a perfectly smooth surface due to the presence of roughness into account.[29] The calculated reflectivity profiles were convoluted with the experimental resolution, assumed to be of Gaussian statistics.

2.5. Grazing Incidence X-ray Diffraction. GIXD was carried out both at beamline BW2 (HASYLAB, Hamburg, see ref 30 for more details) and at 10 keV (λ = 0.124 nm). GISAXS was performed at beamline ID10B[31] (ESRF, Grenoble) using a wavelength of 0.155 nm. Figure 2 shows the general scattering geometry used, which included a scintillation counter as point detector. In both techniques the X-ray beam is incident at the surface of the sample at a small glancing angle below the critical angle of total reflection. Under these conditions only an evanescent wave is generated that propagates along the film−air interface and penetrates into the film with an intensity exponentially decaying with depth. The evanescent wave can be considered as incident beam for 2D X-ray diffraction, giving information about the lateral structure in the plane of the film. The incident angle was set between the critical angles for total reflection of the polymer film and the Si substrate. In this situation the full film thickness contributes to the scattering and the measured signal is maximized. From Figure 2 we note that the X-ray beam impinged along the *x*-axis at an incident angle α_1 and scatters at an exit angle α_2 parallel to the sample surface. The scattering vector was given by $q_x = (2\pi/\lambda)(\cos\psi\cos\alpha_2 - \cos\alpha_1)$, $q_y = (2\pi/\lambda)(\sin\psi\cos\alpha_2)$, and $q_z = (2\pi/\lambda)(\sin\alpha_1 + \sin\alpha_2)$.

3. Results

3.1. Bulk Phase Behavior. SAXS and WAXS were used to determine the bulk phase behavior and to examine the LC ordering of both block copolymers F1 and F2. Figures 3 and 4 show SAXS and WAXS curves, respectively, of the two copolymers at different temperatures. The SAXS curves clearly indicate that both F1 and F2 are microphase separated at all temperatures investigated. The peaks at $q = 0.21$ nm^{-1} in Figure 3a and at $q = 0.32$ nm^{-1} in Figure 3b with corresponding higher-order peaks indicate a cylindrical and a lamellar morphology for copolymers F1 and F2, respectively. The resulting domain sizes *L* are listed in Table 1. Meanwhile, at low temperatures for both block copolymers an additional sharp reflection is observed at $q = 1.89$ nm^{-1}, indicating the presence of smectic layering in the LC domains. This reflection corresponds to a spacing of 3.32 ± 0.10 nm, which is approximately twice the length of the side chain. The smectic layers melt around a temperature of 76 °C for both F1 and F2. The relatively narrow WAXS curve of F1 in Figure 4a indicates that the mesogen layers are partial crystalline at room temperature. The crystalline reflection corresponds to an intermolecular distance of about 0.5 nm between the side chains and is superimposed on a broad amorphous halo. The reflection broadens considerably at a temperature of 72 °C, indicating lateral melting of the crystalline layers. Hence, we assign the room temperature LC phase of copolymer F1 as a crystalline B phase[32] (Cr-B, stacked crystalline layers). The high-temperature LC phase (above 72 °C) is identified as smectic A[32] (Sm-A, stacked liquid layers). In contrast, the WAXS of copolymer F2 in Figure 4b shows only a diffuse peak around 0.5 nm, indicating a Sm-A phase over the full LC range. In agreement with this assignment, the latter peak is best fitted to a Lorentzian. Table 1 summarizes the morphological characteristics and the transition temperatures of the LC phase for both copolymers.

Table 1. Characteristics of the Two Block Copolymers Studied[a]

block copolymer	m	n	Φ_m	T_{BA} (°C)	T_{Ai} (°C)	morphology	L (nm)	q_0 (nm^{-1})	film thickness (nm)
F1	80	74	0.24	72	76	cylindrical	30	0.21	82
F2	79	39	0.35		76	lamellar	20	0.32	146

[a] m and n indicate the degree of polymerization of the PMMA block and the PF8H2A block, repectively; Φ_m is the PMMA volume fraction; T_{BA} and T_{Ai} are the transition temperatures crystalline-B to smectic-A phase and smectic-A to isotropic, respectively.

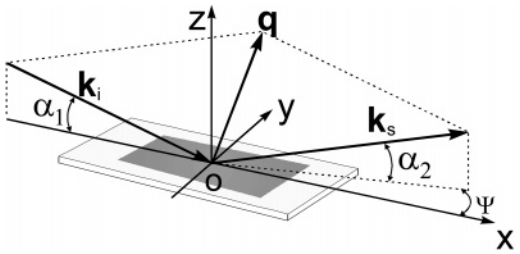

Figure 2. General X-ray diffraction geometry. For XR α_2 and α_1 are varied together keeping $\alpha_2 = \alpha_1$ for $\psi = 0$ leading to $q \equiv q_z$. For GIXD and GISAXS α_1 is set below or close to the critical angle of total reflection. As a result, an evanescent wave is generated, and 2D surface diffraction can be performed by varying ψ for specific choices of α_2.

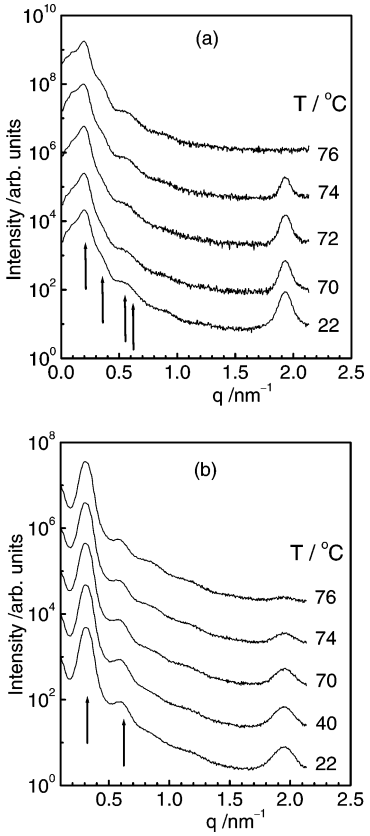

Figure 3. SAXS results at the indicated temperatures. (a) Block copolymer F1, arrows indicate peak positions at a ratio 1:√3 :√7:3. (b) Block copolymer F2, peak positions at a ratio 1:2. Curves have been shifted vertically for clarity.

To determine the relative orientation of the smectic layers with respect to the block copolymer morphology, oriented specimens were prepared by shearing the isotropic melt between two glass slides. Figure 5 displays the resulting SAXS patterns at room temperature. As can be seen, both the cylindrical and the lamellar reflections are orthogonal to the mesogenic reflections. Therefore, in both block copolymers F1 and F2 the smectic layers are perpendicular to the cylindrical and lamellar block interfaces, respectively.

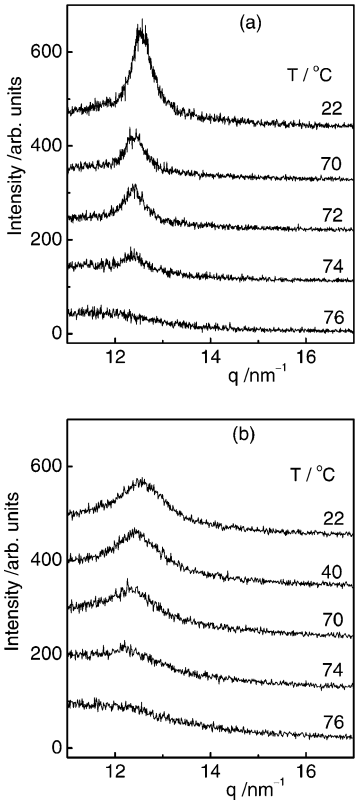

Figure 4. WAXS at the indicated temperatures for (a) block copolymer F1 and (b) block copolymer F2. Curves have been shifted vertically for clarity.

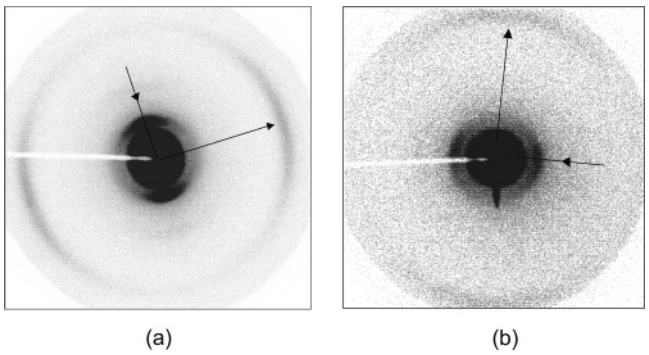

Figure 5. SAXS diffraction patterns at room temperature of an oriented specimen of (a) block copolymer F1 and (b) block copolymer F2. Inward and outward arrows indicate the reflections corresponding to microphase separation and smectic layering, respectively.

3.2. Thin Film Nanostructures. Thin films of both block copolymers were characterized using a combination of XR, AFM, and GIXD. Figure 6 shows typical XR curves of F1 and F2 at room temperature. Note that the reflected intensity has been divided by the Fresnel reflectivity R_F of the Si wafer ($q_c = 0.32$ nm^{-1}) to bring the relevant features clearly out. The two main characteristics of the F1 film of Figure 6a are the high-frequency oscillations that result from interference of the X-rays scattered from the air−film and the film−

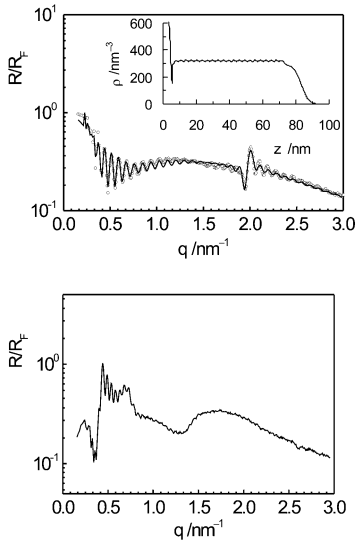

Figure 6. X-ray reflectivity at room temperature of a film of (a) block copolymer F1 and (b) block copolymer F2. The full line in (a) gives the best fit as calculated using the electron density profile in the inset (substrate at $z = 0$).

substrate interfaces (Kiessig fringes) and a Bragg peak at $q = 2.00$ nm^{-1} corresponding to a spacing of 3.14 ± 0.02 nm. No Bragg peaks have been observed at small q values that could be associated with the interdomain period. In the case of an F2 film, displayed in Figure 6b, a much more complex behavior is observed without any discernible Bragg peaks. A quite broad peak is seen around $q = 1.76$ nm^{-1} while a strong beating occurs in the amplitude of Kiessig fringes at low q. In fact, the positions of the "bump" at large q and of the minimum in intensity at low q correspond approximately to the two internal layer periods in the system, smectic layers and block lamellae.

Figure 7 shows AFM images of films of both compounds at room temperature. For the F1 film, cylindrical PMMA domains (dark circular areas) cover the whole area and seem to be oriented normal to the surface but evidently without long-range lateral order. AFM on etched samples indicates that the cylinder penetrate from the surface through the film. Similar AFM images of standing cylinders have been reported by several groups.[11,33] The average diameter of the PMMA cylinders is about 18 nm, and the average center-to-center distance between the cylindrical domains is 33 ± 2 nm. Taking the latter value and assuming perfect cylinders throughout the whole film, on the basis of the volume fraction the cylinder diameter would be around 17 nm. For F2 films a morphology of flat terraces is found with holes of different lateral sizes and an average depth of 20 nm, which is essentially a single block period. This corresponds to the standard situation of a lamellar morphology with the lamellae parallel to the surface.[34−36]

To complement the surface investigations, GIXD and GISAXS (GIXD at small angles) have been be used, which are powerful tools to study the "interior" of soft matter film.[37] Figure 8a,b shows typical GISAXS and GIXD curves of an F1 film. GISAXS gives a peak at $q = 0.207$ nm^{-1}, corresponding to an average lateral periodicity of 30.4 ± 0.05 nm, whereas GIXD shows a peak at $q = 12.44$ nm^{-1}. The latter peak corresponds to a spacing of 0.5 nm, which is consistent with the interchain distance of the side chains in the Cr-B phase, in agreement with the bulk observations. Figure 8c

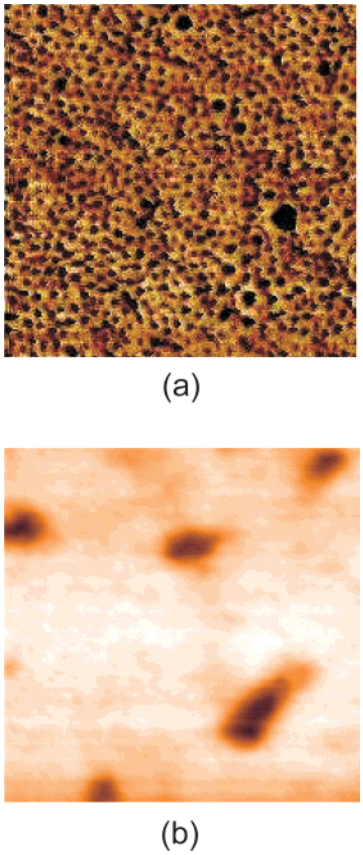

Figure 7. AFM image at room temperature of a film surface of (a) block copolymer F1 (phase image, 1×1 μm^2) and (b) block copolymer F2 (height image, 2×2 μm^2).

shows a GIXD curve of an F2 film at room temperature. A sharp peak at $q = 1.91$ nm^{-1}, characteristic of the mesogenic smectic layers, indicates that the smectic layers are approximately perpendicular to the substrate.

4. Discussion

4.1. Bulk Behavior. The SAXS and WAXS results demonstrate the multilength scale ordering of the two copolymers. The F1 block copolymer microphase separates in hexagonally packed PMMA cylinders in a matrix of a smectic phase, whereas F2 exhibits a lamellar morphology. These results are as expected on the basis of their volume fractions.[35,36] At a smaller length scale, both copolymers show smectic layering with a spacing of 3.33 nm. The fluorinated side chains organize into double layers that do not interpenetrate. In comparison to the interchain distance along the main chain, the diameter of the fluorinated side groups is relative large, which prevents the interdigitation that is often observed for conventional side-chain liquid crystals. The ability of the side chains to crystallize in the smectic layers seems to be influenced by the block morphology. For the cylindrical morphology of F1 the LC phase is continuous (majority block), and the side chains crystallize at low temperatures within the layers, leading to a Cr-B phase. In contrast, for the lamellar morphology of F2 this tendency is suppressed and only a Sm-A phase is observed. Apparently, the continuity of the LC phase is required for a more efficient lateral packing of the fluorinated side chains.

SAXS patterns of oriented samples of both block copolymers samples indicate that the PMMA cylinders in F1 and the block lamellae in F2 are both perpen-

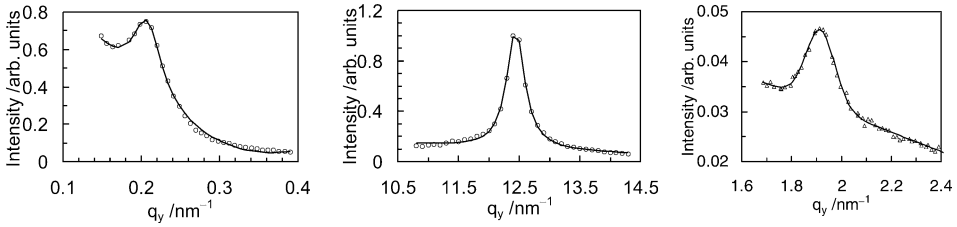

Figure 8. Grazing incident X-ray diffraction results: (a) GISAXS and (b) GIXD of an F1 film; (c) GIXD of an F2 film. Full lines indicate fits to the experimental data as discussed in the text.

dicular to the smectic layers. Such a perpendicular relative orientation has been observed for many lamellar SCLC-BCs. It is attributed to the tendency of the main chain to minimize contact with the amorphous block at the interfaces and depends on the degree of incompatibility between the polymer backbone of the LC block and the amorphous polymer.[14,17]

4.2. Thin Films: Cylindrical Morphology of F1. We start with the XR curve of sample F1 shown in Figure 6a, corresponding to a cylindrical morphology in the bulk. The Kiessig fringes are weak and decay rapidly, indicating a rough surface of the film.[29,38] The periodicity calculated from the discernible Bragg peak around $q = 2.00$ nm^{-1} is very close to the bulk smectic spacing of 3.3 nm. This indicates that the smectic layers are aligned parallel to the substrate with the side chains anchoring to the film interfaces. The best fit to the XR data, given as the continuous line in Figure 6a, indicates a density profile through the film composed of 21 smectic layers with a spacing of 3.2 nm. This regular part of the structure is sandwiched between a monolayer adjacent to the substrate of 1.4 nm thickness and a top layer of 10.3 nm with a considerable roughness (3.7 nm), as shown in the inset of Figure 6a. Assuming the usual situation that the bulk orthogonality of smectic layers and block interfaces is maintained in thin films, the parallel smectic layers point to block domains normal to the film. This is in agreement with the AFM on etched samples. The lateral GISAXS peak at 30.4 nm—very close to the domain period in the bulk (30 nm)—further corroborates this point. Hence, we can safely establish that the cylindrical domains are oriented normal to the substrate. The GISAXS peak can be well fitted by a Lorentzian function with a correlation length of 40 nm. This relatively small value indicates absence of any lateral long-range order in accord with the AFM results. Complementary temperature-dependent AFM reveals that crystallization of the side chains leads to the formation of dendritic superstructures that disappear around 78 °C. These superstructures are at the origin of the large surface roughness of the film surface and might impede lateral long-range order of the cylindrical domains.

On the basis of the above observations, the thin film structure can be represented by the schematic diagram shown in Figure 9a. The PMMA cylindrical domains stand normal to the substrate. The cylindrical domains are embedded in a PF8H2A matrix of which the side chains form smectic bilayers parallel to the substrate. This appears to be the equilibrium structure as annealing the films at 170 °C for more than a week produced no changes in the film structure. The model can be understood in terms of the combined effect of the microphase separation, the orientational wettability of the side chains, and the smectic ordering. The smectic layers have a strong tendency to orient parallel to the interfaces, which effect is reinforced by the orientational

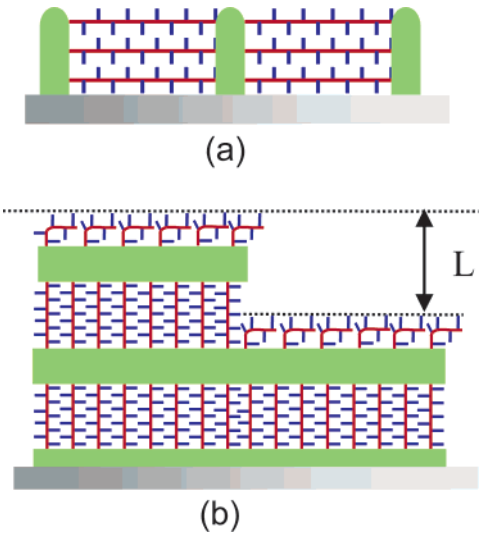

Figure 9. Schematic drawing of the suggested film structures for (a) block copolymer F1 and (b) block copolymer F2. In the first case smectic layers parallel to the film interfaces stabilize perpendicular PMMA cylinders. In the latter model the block lamellae are parallel to the substrate, while the top surface layer is modified allowing optimal interactions of the fluorinated side groups.

wettability of the fluorinated side chains at the surface[39] and—to a lesser extent—also at the substrate. Already above T_{Ai} this can lead to a few surface-induced smectic layers. The microdomain interfaces tend to orient perpendicular to the smectic layers in order to minimize the contact area between the two polymer chains. Hence, we assume that the strong surface interactions suffice already to orient the cylinders perpendicular to the film. Upon cooling below T_{Ai} this initial situation is perfectly suited to accommodate smectic layers parallel to the outer film interfaces throughout the whole film. Note that any alternative of cylinders parallel to the substrate would entail unfavorable contact between the two polymer chains (large enthalpic penalty). In the situation sketched in Figure 9a preferential interactions of the side chains with the air and the substrate and a minimum contact between the two polymer chains (perpendicular relative orientation) can be simultaneously maintained. Whether the fluorinated chains orient homeotropically at the interfaces[40] or have a somewhat tilted orientation[41] cannot be inferred from the present experiments.

In general, for "classical" amorphous block copolymers one can expect cylinders perpendicular to the substrate if the possible gain in surface energy from preferential absorption of one of the blocks is more than compensated by the free energy change associated with the elastic distortions of the chain. This point was nicely demonstrated in the work of Russell and co-workers,[33] who realized films with a perpendicular orientation of cylinders by making the substrate neutral to both blocks

via coating with a random copolymer. In the case of a smectic LC block as majority component the anchoring of the mesogens provides the driving force to orient smectic layers parallel to substrate and surface and thus the block interfaces perpendicular. The fluorinated groups present in this work reinforce this effect by their strong surface anchoring.

4.3. Thin Films: Lamellar Morphology of F2. Increasing the volume fraction of the PMMA block evidently has considerable consequences on the thin film morphology. The flat terrace structure revealed by AFM indicates a typical parallel lamellar morphology. In fact, incomplete top layers seen in AFM and/or XR have become a kind of benchmark for identifying parallel lamellae.[34−36] This suggests a simple structure with a PMMA layer wetting the substrate and block lamellae parallel to the film interfaces. This idea is supported by the observation of a smectic peak in the GIXD curve of Figure 8c, which indicates that a large fraction of the smectic layers are perpendicular to the substrate as opposed to parallel layers in the case of F1. Hence, in thin films of F2 again a perpendicular orientation of the bulk smectic layers relative to the lamellar block morphology is found. However, the XR results contradict such a simple lamellar structure parallel to the substrate, and attempts to fit the XR curve in this way were not successful. The broad peak around $q = 1.76$ nm^{-1} indicates a hybrid structure that is more evolved. We attribute this feature qualitatively to a top layer with locally smectic layers parallel to the surface. The rudimentary Bragg peak at low q values corresponds to the lamellar domain period. Fitting this part of the XR curve is compatible with the basic parallel lamellar model. The curious behavior of the phase of the XR intensity is probably caused by the specific termination of this structure at the transition to the top layer. Combination of these elements leads to the tentative model depicted in Figure 9b.

In agreement with the discussion above for block copolymer F1, we assume again strong surface interactions of the fluorinated chains, giving above T_{Ai} smectic boundary layers at the air interface. The natural extension of this reasoning in terms a perpendicular relative orientation of block interfaces and smectic layers would lead to a structure of block lamellae perpendicular to the substrate. In fact, such structures have been observed by Wong et al.[16] In contrast to the situation for compound F1—in which PMMA is the minority component—now the preference of PMMA for the substrate leads to a parallel PMMA layer that is not compatible with such a structure. Meanwhile, a perpendicular relative orientation of smectic layers and block lamellae is maintained in the "bulk" of the film, which requires a hybrid structure with a changing orientation of the fluorinated top layer. Details of the transition cannot be inferred from the present experiments because we have not been able to fit the XR data in some detail. Note that in standard lamellar block copolymer films the enthalpic contribution to the free energy is small and entropic contributions dominate.[42] Evidently this is not true in our case of strongly interacting fluorinated chains.

5. Conclusions

The fluorinated side-chain liquid-crystalline diblock copolymers investigated show a strong tendency to surface organization because of the intrinsic low surface energy of the fluorinated side groups. In the bulk both block copolymers exhibit a smectic phase with the side chains organized in double layers. In thin films of the cylinder-forming block copolymer, cylindrical PMMA domains normal to the substrate are obtained, but only ordered over a limited correlation length. The combination of smectic layering within the LC domains and orientational wettability of the side chains stabilizes the minority cylindrical domains normal to the film. For the lamellae-forming block copolymer, a hybrid lamellar structure is formed in which the block lamellae are basically parallel to the substrate in combination with a rearrangement of the top layer in order to satisfy the mesogenic anchoring requirements.

Acknowledgment. The authors thank B. I. Ostrovskii for helpful discussions and K. Albrecht for her assistance with the AFM measurements. This work is supported in part by the European Community's Human Potential Program under Contract HPRN-CT-1999-00151 (POLYNANO) and is part of the research program of the "Stichting voor Fundamenteel Onderzoek der Materie (FOM)", which is financially supported by the "Nederlandse Organisatie voor Wetenschappelijk Onderzoek (NWO)". M. Al-Hussein and Y. Séréro acknowledge financial support provided through POLYNANO.

References and Notes

(1) Walther, M.; Finkelmann, H. *Prog. Polym. Sci.* **1996**, *21*, 951.
(2) Mao, G.; Ober; C. K. *Acta Polym.* **1997**, *48*, 405.
(3) Poser, S.; Fischer, H.; Arnold, M. *Prog. Polym. Sci.* **1998**, *23*, 1337.
(4) Adams, J.; Gronski, W. *Macromol. Chem., Rapid Commun.* **1989**, *10*, 553.
(5) Fischer, H.; Poser, S.; Arnold, M.; Frank, W. *Macromolecules* **1994**, *27*, 7133.
(6) Bohnert, R.; Finkelmann, H. *Macromol. Chem. Phys.* **1994**, *195*, 689.
(7) Yamada, M.; Iguchi, T.; Hirao, A.; Nakahama, S.; Watanabe, J. *Macromolecules* **1995**, *28*, 50.
(8) Mao, G.; Wang, J.; Clingman, S. R.; Ober, C. K.; Chen, J. T.; Thomas, E. L. *Macromolecules* **1997**, *30*, 2556.
(9) Sänger, J.; Gronski, W.; Maas, S.; Stühn, B.; Heck, B. *Macromolecules* **1997**, *30*, 6783.
(10) Anthamatten, M.; Hammond, P. T. *Macromolecules* **1999**, *32*, 8066.
(11) Figueiredo, P.; Geppert, S.; Brandsch, R.; Bar, G.; Thomann, R.; Spontak, R. J.; Gronski, W.; Samlenski, R.; Müller-Buschbaun, P. *Macromolecules* **2001**, *34*, 171.
(12) Ansari, I. A.; Castelletto, V.; Mykhaylyk, T.; Hamley, I. W.; Lu, Z. B.; Itoh, Y.; Imrie, C. T. *Macromolecules* **2003**, *36*, 8898.
(13) Lee, M.; Cho, B.; Zin, W. *Chem. Rev.* **2001**, *101*, 3669.
(14) de Jeu, W. H.; Séréro, Y.; Al-Hussein, M. *Adv. Polym. Sci.* **2005**, *181*, 75.
(15) Fasolka, M. J.; Mayes, A M. *Annu. Rev. Mater. Res.* **2001**, *31*, 323.
(16) Wong, G. C. L.; Commandeur, J.; Fischer, H.; de Jeu, W. H. *Phys. Rev. Lett.* **1996**, *77*, 5221.
(17) Sentenac, D.; Demirel, A. L.; Lub, J.; de Jeu, W. H. *Macromolecules* **1999**, *32*, 3235.
(18) Hare, E. F.; Shafrin, E. G.; Zisman, W. A. *J. Phys. Chem.* **1954**, *58*, 236.
(19) Katano, Y.; Tomono, H.; Nakajima, T. *Macromolecules* **1994**, *27*, 2342.
(20) Krupers, M.; Möller, M. *Macromol. Chem. Phys.* **1997**, *198*, 2163.
(21) Wang, J.; Mao, G.; Ober, C. K.; Edward, J. K. *Macromolecules* **1997**, *30*, 1906.
(22) Krupers, M.; Slangen, P.-J.; Möller, M. *Macromolecules* **1998**, *31*, 2558.
(23) Xiang, M.; Li, X.; Ober, C. K.; Char, K.; Genzer, J.; Sivaniah, E.; Edward, J. K.; Fisher, D. A. *Macromolecules* **2000**, *33*, 6119.
(24) Andruzzi, L.; Chiellini, E.; Galli, G.; Li, X.; Kang, H. K.; Ober, C. K. *J. Mater. Chem.* **2002**, *12*, 1684.

(25) Li, X.; Andruzzi, L.; Chiellini, E.; Galli, G.; Ober, C. K.; Hexemer, A.; Edward, J. K.; Fisher, D. A. *Macromolecules* **2002**, *35*, 8087.
(26) Osuji, C.; Ferreira, P. J.; Mao, G.; Ober, C. K.; Sande, J. B. V.; Thomas, E. L. *Macromolecules* **1997**, *30*, 1906.
(27) Yokoyama, H.; Tanaka, K.; Takahara, A.; Kajiyama, T.; Sugiyama, K.; Hirao, A. *Macromolecules* **2004**, *37*, 939.
(28) Urushihara, Y.; Nishino, T. *Langmuir* **2005**, *21*, 2614.
(29) See, for example: Tolan, M. *X-ray scattering from Soft Matter Thin Films*; Springer: Berlin, 1999.
(30) de Jeu, W. H.; Fera, A.; Ostrovskii, B. I. *Eur. Phys. J. E* **2004**, *15*, 61.
(31) Smilgies, D. M.; Boudet, N.; Struth, B.; Konovalov, O. *J. Synchrotron Rad.* **2005**, *12*, 329.
(32) See, for example: Vertogen, G.; de Jeu, W. H. *Thermotropic Liquid Crystals, Fundamentals;* Springer: Berlin, 1988.
(33) (a) Mansky, P.; Liu, Y.; Huang, E.; Russell, T. P.; Jaeger, H. M. *Science* **1997**, *275*, 1458. (b) Lin, Z. Q.; Kim, D. H.; Wu, X. D.; Boosahda, L.; Stone, D.; LaRose, L.; Russell, T. P. *Adv. Mater.* **2002**, *14*, 1373.
(34) Coulon, G.; Collin, B.; Ausseré, D.; Chatenay, D.; Russell, T. P. *J. Phys. (Paris)* **1990**, *51*, 2801.
(35) Bates, F. M.; Fredrickson, G. H. *Annu. Rev. Phys. Chem.* **1990**, *41*, 525.
(36) Hamley, I. W. *The Physics of Block Copolymers*; Oxford University Press: New York, 1998.
(37) See for example: (a) Busch, P.; Smilgies, D. M.; Posselt, D.; Kremer, F.; Papadakis, C. M. *Macromol. Chem. Phys.* **2003**, *204*, F18. (b) Mueller-Buschbaum, P. *Anal. Bioanal. Chem.* **2003**, *376*, 3. (c) Xu, T.; Goldbach, J. T.; Misner, M. J.; Kim, S.; Gibaud, A.; Gang, O.; Ocko, B.; Guarini, K. W.; Black, C. T.; Hawker, C. J.; Russell, T. P. *Macromolecules* **2004**, *37*, 2972. (d) Lee, B.; Park, I.; Yoon, J.; Park, S.; Kim, J.; Kim, K.-W.; Chang, T.; Ree, M. *Macromolecules* **2005**, *38*, 4311.
(38) Russell, T. P. *Mater. Sci. Rep.* **1990**, *5*, 171.
(39) Wu, S. H. *Polymer Interfaces and Adhesion*; Marcel Dekker: New York, 1982.
(40) Mourran, A.; Tartsch, B.; Gallyamov, M.; Magnov, S.; Lambreva, D. M.; Ostrovskii, B. I.; Dolbnya, I.; de Jeu, W. H.; Moeller, M. *Langmuir* **2005**, *21*, 2308.
(41) Li, X.; Andruzzi, J.; Chiellini, E.; Galli, G.; Ober, C. K.; Hexemer, A.; Kramer, E. J.; Fischer, D. A. *Macromolecules* **2002**, *35*, 8078.
(42) See, for example: Busch, P.; Posselt, D.; Smilgies, D.-M.; Reinlaender, B.; Kremer, F.; Papadakis, C. M. *Macromolecules* **2003**, *36*, 8717.

MA050972X